Ethanol conversion into 1,3-butadiene over a mixed Hf-Zn catalyst: a study of the reaction pathway and catalyst deactivation

G. M. Cabello González[1], R. Murciano[2], A. L. Villanueva Perales[1*], A. Martínez[2], F. Vidal-Barrero[1], M. Campoy[1]

[1] Departamento de Ingeniería Química y Ambiental, Escuela Técnica Superior de Ingeniería, Universidad de Sevilla, Camino de los Descubrimientos, s/n. 41092 Sevilla, Spain.

[2] Instituto de Tecnología Química, Universitat Politècnica de València - Consejo Superior de Investigaciones Científicas (UPV-CSIC), Avda. de los Naranjos s/n, 46022 Valencia, Spain.

* Corresponding author. Email: angelluisvp@us.es

Departamento de Ingeniería Química y Ambiental, Escuela Técnica Superior de Ingeniería, Universidad de Sevilla, Camino de los Descubrimientos, s/n. 41092 Sevilla, Spain.

Abstract

Some fundamental and practical aspects of a Hf-Zn catalyst, with a nominal composition of 3.0 wt% Hf and 9.3 wt% Zn and prepared as a physical mixture of Hf/SiO_2 (85 wt%) and the zinc-silicate hemimorphite (15 wt%), have been studied for the one-step conversion of ethanol to 1,3-butadiene. The elucidation of the main reactions leading to 1,3-butadiene and by-products was made by means of kinetic curves and catalytic tests where intermediates were individually fed. In addition, the convenience of by-product separation from unreacted ethanol in an industrial process was studied by performing experiments where ethanol was co-fed with intermediates. The causes of catalyst deactivation and the impact on catalyst structure and performance of regeneration by calcination were also investigated. According to our results, the pathway to 1,3-butadiene over the Hf-Zn catalyst includes ethanol dehydrogenation, acetaldehyde aldol condensation, crotonaldehyde reduction with ethanol, and crotyl alcohol dehydration. The recycling of the by-products butanal, acetone and 1-butanol into the reactor should be avoided, as the first two are converted to heavy compounds by aldol condensation reactions, while 1-butanol dehydration leads to butenes, which are difficult to separate from 1,3-butadiene. The suppression of diethyl ether formation from ethanol by recycling to extinction is possible. It has been found that catalyst deactivation is mainly caused by the retention of oxygenated aromatic-type coke species, preferentially formed on the dehydrogenating Zn^{2+} sites associated with the hemimorphite component of the catalyst, and probably also by a loss in Zn^{2+} sites due to the reduction to Zn^0 during catalysis. This reduction induces an imbalance between Hf^{4+} and Zn^{2+} sites, which changes catalyst selectivity. Regeneration by calcination with air removes coke and re-oxidizes a fraction of Zn^0 back to Zn^{2+}, but it does not fully re-establish the original Zn^{2+}/Hf^{4+} balance.

Keywords: Ethanol; 1,3-butadiene; hafnium-zinc catalyst; reaction pathway; deactivation-regeneration.

1. Introduction

1,3-Butadiene is an important building block for the manufacture of synthetic rubber, resins, and elastomers [1] and it is mostly produced as a by-product of the naphtha or gas oil steam cracking process. In recent years, due to the recent shale gas revolution, the increasing use of ethane as steam cracking feedstock instead of heavier fractions has caused a decrease in the production of 1,3-butadiene, even though its demand continues to grow at a rate of 1-2% per year. Therefore, the short-term demand for 1,3-butadiene is not expected to be satisfied by the current capacity of oil refineries [2,3]. In that context, the production of 1,3-butadiene from renewable sources, such as bioethanol, is receiving increasing attention as an environmentally friendly alternative to fulfil the demand gap while contributing to mitigate CO_2 emissions. Moreover, bioethanol is currently the largest biofuel on the market and its production is expected to continue to grow in the future [4-6].

The process to catalytically convert ethanol into 1,3-butadiene was industrially born in the 20th century around the time of the Second World War. The so-called Lebedev's process in the former USSR was the first industrial process to produce 1,3-butadiene directly from ethanol using a $MgO\text{-}SiO_2$ catalyst. Later, in the USA, the Union Carbide and Carbon Chemicals Corporation started the manufacture of 1,3-butadiene from ethanol based on the Ostromislensky two-step process. In the first step of this process, acetaldehyde is generated by ethanol dehydrogenation, while the second step involves the conversion of the acetaldehyde/ethanol mixture into 1,3-butadiene over a Ta_2O_5/SiO_2 catalyst [3]. However, these technologies were abandoned around 1960 due to a lack of competitiveness against the petrochemical route [7-12]. Therefore, the development of novel catalytic materials with improved activity and selectivity

becomes essential to improve the techno-economic viability of the ethanol-to-1,3-butadiene process.

The present study focuses on the direct or one-step process. Modifications to the traditional MgO/SiO_2 one-step catalyst aiming to improve its performance have been proposed in the literature [3,7], such as modifying the properties of the silica support and/or the preparation method [13-17]. Addition of a transition metal and/or replacement of MgO with one or more transition metal oxides has also been thoroughly studied [1,4,8-10,18-24]. On this regard, this work is based on the study by De Baerdemaeker et al. [25] on silica-supported catalysts of bimetallic mixtures of Hf(IV)-Zn(II) and trimetallic mixtures of Cu(II)-Hf(IV)-Zn(II) and Cu(II)-Zr(IV)-Zn(II). For those systems, they investigated the effect of the preparation method and metal source and found that the system Hf(IV)-Zn(II) provided the highest butadiene yield (60-70%) when hemimorphite, a crystalline zinc silicate ($Zn_4Si_2O_7(OH)_2 \cdot H_2O$), is used as the source of Zn and then physically mixed with HfO_2/SiO_2. Therefore, as a promising catalyst for the conversion of ethanol into 1,3-butadiene, the present work aims to study aspects of the Hf(IV)-Zn(II) catalyst which are relevant for its industrial application, such as the reaction pathway to elucidate the effect of recycling by-products to the reactor and the catalyst deactivation/regeneration behaviour.

Although significant research has been carried out in the past to elucidate the reaction pathway of the one-step conversion of ethanol to 1,3-butadiene, this is still a subject of controversy due, most probably, to differences in the type of catalyst and/or reaction conditions employed in these studies. Nonetheless, the most widely accepted reaction pathway considers crotonaldehyde as a key intermediate [26-28] and comprises, as main steps, the ethanol dehydrogenation to acetaldehyde, the aldol condensation of acetaldehyde to 3-hydroxybutanal,

the dehydration of 3-hydroxybutanal to crotonaldehyde, the selective reduction of crotonaldehyde by ethanol to crotyl alcohol through the Meerwein-Ponndorf-Verley-Oppenauer (MPVO) reaction, and the dehydration of crotyl alcohol to 1,3-butadiene. ZnO-Al_2O_3 and MgO-SiO_2 have been the catalytic systems most commonly studied to unveil this pathway [26-35]. Recently, for the first time, a detailed reaction mechanism based on this pathway was proposed for a one-step Ag-ZrO_2-SiO_2 catalyst by using information derived from kinetic measurements and tracing techniques [29]. The main criticism against the aldol condensation reaction pathway is that crotonaldehyde is found in trace amounts while 3-hydroxybutanal is not detected at all in the reaction products. In this regard, some researchers argue that 3-hydroxybutanal is not observed because it is very reactive and is rapidly dehydrated to crotonaldehyde once it is formed [9,27,30,31,36,37]. Besides the aldol condensation pathway, others routes for the one-step conversion of ethanol to 1-3 butadiene have been proposed in the literature [15,38,39].

Regardless of the catalytic system used, side products are always formed along with 1,3-butadiene. The quantity and nature of these side products depend not only on the reaction conditions, but also on the catalyst studied and are not usually mentioned in the literature. This issue is of paramount importance from the viewpoint of process design for selecting the appropriate technologies in the separation train. In addition, the reactions where side products are involved should be clarified in order to anticipate the effect of recycling some of these compounds back into the reactor. Makshina et al. [3] summarized all the studies by Quattlebaum and Gorin et al. regarding the main side products formed in the conversion of ethanol to 1,3-butadiene over Ta_2O_5/SiO_2 and MgO-SiO_2 catalysts. Setting aside the catalytic system, the main side products reported in the literature are ethene and diethyl ether, directly produced by ethanol dehydration, and butenes. In addition, ethyl acetate, butanal, n-butanol, acetone, propene, CO_2

and CO are also typically formed, albeit in lesser amounts. At high ethanol conversions, heavy polar and non-polar compounds (grouped as C_{6+}) are also usually produced [7,8,15,20,23,25,32,40-45].

The deactivation of the catalyst during the ethanol-to-1,3-butadiene reaction is an important aspect to be considered as well. It is well known from the literature that the commercial catalysts previously used in the one- and two-step processes suffered from a fast deactivation that is believed to be due to coke deposition and, thus, regeneration was required to recover their initial activity [27,28]. In spite of its relevance for the catalyst/process design, very few studies have reported on the deactivation and regeneration of new catalytic systems developed for this reaction. For instance, the deactivation of silica-supported bi- and tri-metallic catalysts was related to pore blockage and, accordingly, its extent was lowered by increasing the pore size of the silica support [9]. Similarly, Chae et al. [40] observed a lower deactivation for Ta_2O_5/SiO_2 catalysts when using an ordered mesoporous silica (OMS) as support instead of a commercial silica. Catalyst regeneration by calcination resulting in full recovery of the catalyst activity has been reported by Chae et al. for Ta_2O_5/OMS after one regeneration cycle and by Cheong et al. [46] for zirconium oxide supported on mesocellular siliceous foam after two regeneration cycles. In other cases, however, the regeneration failed for unknown reasons. For instance, although regeneration studies with Na-doped Zn-Zr mixed-metal oxides [23] revealed the recovery of their initial activity, the deactivation rate was seen to double after regeneration. On the other hand, Simoni da Ros et al. [44] reported that regeneration by calcination of a K_2O:ZrO_2:ZnO/MgO-SiO_2 catalyst did not fully restore the catalyst activity. Unfortunately, even if these observations might point towards a change in the catalyst structure during the

regeneration process, no studies addressing this issue have been reported so far for one-step catalytic systems.

Based on the above premises, in this work we performed a kinetic study to derive, for the first time, a detailed reaction pathway leading to 1,3-butadiene as well as to intermediate and side products over the Hf-Zn catalyst. This catalytic system was selected for its high yield and selectivity to 1,3-butadiene [25]. Next, the deactivation and the regeneration behaviour of the catalyst were investigated. The likely causes of deactivation and of the changes in catalytic performance observed upon regeneration by air calcination are discussed based on the characterization of the Hf-Zn catalyst at different stages (fresh, used, and regenerated) employing a set of techniques, including TGA-DTG, GC-MS, ^{1}H-to-^{13}C CP-MAS NMR, XRD, STEM-EDX, and XPS.

2. Experimental

2.1. Catalyst preparation

The Hf-Zn catalyst employed in this study, with a nominal composition of 3.0 wt% Hf and 9.3 wt% Zn, was prepared according to a methodology similar to that described for the sample denoted as $Hf_{3.0}Zn_{9.3}$ (Table 3, entry 6) in the work by De Baerdemaeker et al. [25]. Briefly, the zinc silicate hemimorphite ($Zn_4Si_2O_7(OH)_2 \cdot H_2O$, abbreviated as HM) was first synthesized by precipitation at a pH of ca. 7 using a commercial aqueous Na_2SiO_3 solution (26.8 wt% SiO_2, 10.6 wt% Na_2O, 62.6 wt% H_2O, Sigma-Aldrich) and $Zn(NO_3)_2 \cdot 6H_2O$ (Sigma-Aldrich, 98% purity) as silicon and zinc sources, respectively. Concurrently, a Hf/SiO_2 solid was prepared by wet impregnation (liquid/solid ratio of 20 cm^3/g) of a commercial silica (Cab-O-Sil M5, Cabot Corporation) with an aqueous solution containing the required amount of $HfCl_4$

precursor (Acros Organics, 99% purity) to achieve a nominal Hf loading of 3.5 wt%. After elimination of the water solvent in a rotary evaporator, the solid was dried at 100 ºC for 12 h and subsequently calcined in flowing air at 500 ºC for 4 h (heating rate of 1 ºC/min). The final catalyst, hereafter denoted within the text as Hf-Zn, was then produced by physically mixing the HM and Hf/SiO_2 components in the appropriate proportions (85 wt% Hf/SiO_2, 15 wt% HM) to achieve the desired nominal metal composition (3.0 wt% Hf, 9.3 wt% Zn).

2.2. Characterization methods

The content of Hf and Zn in the calcined catalyst was determined by Inductively Coupled Plasma-Optical Emission Spectrometry (ICP-OES) in a Varian 715-ES spectrometer prior to digestion of the solid in an acid mixture of HNO_3:HF:HCl (1:1:3 volume ratio). Crystalline phases in the materials were identified by powder X-ray diffraction (XRD) in a Panalytical Cubix Pro diffractometer equipped with a graphite monochromator operating at 40 kV and 45 mA using nickel-filtered CuK_α radiation (λ= 0.1542 nm). The textural properties of the individual HM and Hf/SiO_2 solids and the Hf-Zn catalyst were measured by N_2 physisorption at liquid N_2 temperature (-196 °C) in a Micromeritics ASAP-2420 equipment. Prior the analyses, the samples were degassed at 300 °C under vacuum overnight. The element distribution in fresh, spent, and regenerated catalyst samples was obtained by energy-dispersive X-ray spectroscopy (EDX) using an Oxford INCA Energy 2000 system coupled to a 200 kV JEOL JEM-2100F microscope operating in scanning-transmission mode (STEM). The composition and nature of the Hf, Zn, and C species present on the catalyst surface were studied by X-ray photoelectron spectroscopy (XPS). XP spectra were recorded in a VG-Escalab-210 spectrometer using Al K_α

radiation (1486.6 eV) and a pass energy of the analyzer of 30 eV. Charge correction of the XP spectra was made based on the Si2p peak located at 103.5 eV.

The acidity of the calcined Hf-Zn catalyst and its components (HM, Hf/SiO_2) was studied by FTIR spectroscopy of adsorbed pyridine in a Nicolet 710 FTIR spectrometer using self-supported wafers (10 mg/cm^2). Complementary characterization by low-temperature FTIR of CO adsorption was performed to investigate in more detail the different types and strength of the Brønsted and Lewis acid sites present on the surface of the Hf-Zn catalyst and its components (HM and Hf/SiO_2). Since the extinction coefficients of CO adsorbed on Brønsted and Lewis acid sites in these materials are unknown, preventing quantification of the different types of acid sites, the results of the FTIR-CO measurements will be discussed on a qualitative basis.

Solid-state ^{1}H-to-^{13}C cross-polarization (CP) MAS NMR spectroscopy was performed to study the nature of the carbon compounds deposited on the catalyst during the reaction. The $^{1}H/^{13}C$ CP-MAS NMR spectrum was recorded at room temperature on a Bruker AV III HD 400 WB spectrometer at a spinning ratio of 5 kHz with a 90º pulse for ^{1}H of 5 μs, a contact time of 3.5 ms, and a recycle delay of 5 s. The ^{13}C spectrum was referred to adamantane.

Thermogravimetric analysis (TGA-DTG) of the spent catalyst was performed in a Metler Toledo TGA/SDTA 851E analyzer under flowing air by linearly increasing the temperature from 50 to 800 ºC at a rate of 10 ºC/min. The total amount of carbon in the spent and regenerated catalyst was determined by elemental analysis in a Fisons Inst. EA1108 CHNS-O analyzer. The nature of the carbon species present in the spent sample was assessed by mass spectrometry (MS) after dissolving the solid in HF and subsequent extraction of the soluble coke species with CH_2Cl_2.

Further details of the experimental conditions employed in some of the above characterization techniques are given in Supporting Information.

2.3. Experimental facility and catalytic tests

Catalytic tests were carried out in a continuous flow fixed-bed reactor at 360 ºC and atmospheric pressure. Prior to reaction, the catalyst was pressed, crushed, and sieved to collect the 0.3-0.5 mm fraction. The internal diameter of the stainless steel tube reactor was 0.83 cm and its length 25.8 cm. The bed was divided into three sections. The top section was a SiC bed of 8 cm, the middle one comprised a bed of catalyst diluted in the necessary amount of SiC to obtain a bed length of 13 cm, and the bottom section was also a SiC bed. All sections were separated by a glass wool plug. The reactor output line was electrically traced at around 300 ºC and insulated to avoid product condensations before analysis by on-line gas chromatography (GC). The online analyses were performed in an Agilent 7890A gas chromatograph equipped with two flame ionization detectors (FID), one for C_1-C_6 hydrocarbons and the other one for oxygenated compounds (alcohols, aldehydes, ketones...), and a thermal conductivity detector (TCD) for the separation and quantification of other compounds such as CO, CO_2, H_2, N_2, H_2O, etc. The start-up procedure is detailed in Supporting Information.

Kinetics curves were obtained by carrying out several tests on the Hf-Zn catalyst at 360 ºC, varying the space velocity (WHSV) from 1.12 to 50 h^{-1} by changing either the amount of catalyst or the ethanol flow rate so as to cover a wide range of ethanol conversions. Additional experiments were carried out where relevant intermediate reaction products were individually fed or co-fed in different ratios with ethanol to better understand their contribution in the overall

reaction scheme. The conditions employed in the catalytic tests using single and co-fed reactants are summarized in Tables 1 and 2, respectively, and further explained in Supporting Information.

Table 1. Single reactant tests. All tests were carried out at 360 ºC and atmospheric pressure.

Feedstock	WHSV (h^{-1})	Reactant Partial Pressure (bar)
Ethanol (Panreac, 99.8%)	1.12-50	0.21
Acetaldehyde (Sigma-Aldrich, 99.5%)	1.12-9.8	0.21
Crotonaldehyde (Sigma-Aldrich, 99.5%)	6.1	0.21
Crotyl alcohol (Sigma-Aldrich, 96%)	1.12	0.04
1,3-Butadiene (Air Liquide, 20% in N_2)	1.3-0.65	0.04
1-Butanol (Indukern, 98%)	9-30	0.21
Acetone (Merck, 99.8%)	1.12	0.21
Butanal (Sigma-Aldrich, 99%)	1.12	0.21

Table 2. Co-feeding tests. All tests were carried out at 360 ºC and atmospheric pressure.

Feedstock	WHSV (h^{-1})	Ethanol Partial Pressure (bar)	Concentration of intermediate in ethanol (wt%)
Ethanol + Diethyl Ether (Sigma-Aldrich, 99.5%)	1.12	0.21	2.5, 5, 10
Ethanol + Butanal	1.12	0.21	2.5, 5, 10
Ethanol + Acetone	1.12	0.21	2.5, 5, 10
Ethanol + Crotonaldehyde	9.8	0.21	5, 10
Ethanol + 1,3-Butadiene	3.2	0.21	3.2

Finally, a test lasting 100 h was done to assess the deactivation behaviour of the catalyst at WHSV of 1.12 $g_{EtOH}/(g_{cat}\cdot h)$, T= 360 ºC, P_{EtOH} of 0.21 bar, and P_{total} of 1 bar. During the test, the catalyst was submitted to two in-situ regeneration cycles by calcination at 500 ºC in flowing air (15 cm^3/min). The first regeneration lasted 6 h and was initiated once the catalyst lost ca. 20% of its initial conversion (corresponding to a time on stream (TOS) of 35 h). The second regeneration cycle, starting at a TOS of ca. 60 h, was also performed by air calcination at 500 ºC and lasted 8 h. After each regeneration cycle, the evolution with TOS of the catalytic performance was followed in order to study the consequences of deactivation and regeneration on the activity and product yield/selectivity of the Hf-Zn catalyst.

The reactant conversion and the selectivity and yield (both expressed on a carbon basis) to a given product were defined in Eq. 1.1-1.3.

$$Conversion\ (\%) = \frac{Converted\ reactant\left(\frac{mmol}{min}\right)}{Fed\ reactant\ \left(\frac{mmol}{min}\right)} \bullet 100 \qquad (1.1)$$

$$Selectivity\ (\%) = \frac{C\ atoms\ to\ product\left(\frac{mmol}{min}\right)}{C\ atoms\ in\ all\ products\ \left(\frac{mmol}{min}\right)} \bullet 100 \qquad (1.2)$$

$$Yield\ (\%) = \frac{Conversion\ (\%) \bullet Selectivity(\%)}{100} \qquad (1.3)$$

For single reactant tests the weight hourly space velocity (WHSV) was defined in Eq. 1.4 as the mass flow rate of the reactant divided by the mass of catalyst in the reactor. Only the mass flow of ethanol was considered for calculating WHSV in co-feeding tests. Carbon mass balance errors for the experiments reported in this study were below 10%.

$$WHSV(h^{-1}) = \frac{mass flow\ of\ reactant\ feed\left(\frac{g}{h}\right)}{load\ of catalyst(g)} \quad (1.4)$$

3. Results and discussion

3.1. Physicochemical properties of the materials

The commercial silica employed as support in the preparation of the Hf/SiO_2 component presented the following textural parameters: BET area of 212 m^2/g, total pore volume of 1.30 cm^3/g, and mean pore diameter of 26 nm. The results of the N_2 physisorption measurements for the individual HM and Hf/SiO_2 solids and the Hf-Zn catalyst are gathered in Table 3. As seen there, the textural properties of the Hf/SiO_2 solid showed minor deviations with respect to those of the bare SiO_2 support, as expected from the low Hf loading (3.5 wt%). In comparison, the hemimorphite (HM) exhibited much lower BET surface area and total pore volume albeit higher average pore size. On the other hand, the Hf-Zn catalyst, prepared by physically mixing Hf/SiO_2 and HM, displayed values of the textural properties which are intermediate to those of the individual components, although much closer to the Hf/SiO_2 solid, as anticipated by considering the mass proportion of each component in the physical mixture (85 wt% Hf/SiO_2 + 15 wt% HM)

Table 3. Textural properties of the individual HM (hemimorphite) and Hf/SiO_2 solids and the Hf-Zn catalyst as measured by N_2 physisorption.

Sample	BET area (m^2/g)	Total pore volume (cm^3/g)	Mean pore diameter (nm)
Hf/SiO_2	206	1.26	26
HM	51	0.46	42
Hf-Zn	179	1.10	28

The XRD patterns of the hemimorphite (HM), the impregnated and calcined Hf/SiO_2 solid, and the final Hf-Zn catalyst are presented in Fig. S1 (Supporting Information). The synthesized HM sample exhibits only the characteristic diffractions for hemimorphite (JCPDS 5-0555), and confirms its successful preparation and high purity. On the other hand, the absence of reflections related to Hf compounds in the Hf/SiO_2 component evidences its high dispersion on the amorphous SiO_2 carrier. The Hf-Zn catalyst shows only the X-ray diffractions associated to the hemimorphite phase, albeit with a much attenuated intensity with respect to pure hemimorphite, as expected by its high dilution with Hf/SiO_2 in the physical mixture. According to repeated ICP-OES analyses, the Hf and Zn contents in the catalyst are, respectively, 2.5 (±0.1) wt% and 10.0 (±1.0) wt%, which are close to the nominal values. A representative STEM image and the element EDX mapping for Si and Zn in the fresh Hf-Zn sample are shown in Fig. S2. The brightest regions in the STEM image clearly correspond to Zn species in the hemimorphite (corroborated by EDX) which appears as a separate phase in the physically mixed catalyst, as expected.

The acid properties of hemimorphite (HM), Hf/SiO_2, and Hf-Zn catalyst were first assessed by FTIR spectroscopy of adsorbed pyridine. The respective FTIR-pyridine spectra at a desorption temperature of 150 °C are compared in Fig. 1. According to this technique, the Hf-Zn catalyst, as well as its components, exhibit essentially Lewis-type acidity, as characterized by the IR band at ca. 1450 cm^{-1}. The somewhat lower frequency of this band in Hf/SiO_2 and Hf-Zn catalyst (1449 cm^{-1}) compared to HM (1452 cm^{-1}) might suggest that the Lewis acid sites associated with Zn^{2+} species in hemimorphite are of a slightly higher strength than those related to Hf^{4+} sites. Moreover, the presence of a shoulder at 1452 cm^{-1} besides the main peak at 1449 cm^{-1} in the spectrum of the Hf-Zn catalyst (spectrum c) indicates that both Zn^{2+} and Hf^{4+} species

contribute to its total Lewis acidity. The concentration of Lewis acid sites amounts to 65, 39, and 41 μmol/g for HM, Hf/SiO_2, and Hf-Zn catalyst, respectively. These results indicate that the Lewis acidity of the catalyst is mostly determined by that of its main component Hf/SiO_2. Moreover, the absence of a band at ca. 1545 cm^{-1} in all three samples indicates that the amount of Brønsted acid sites, if present, should be very low and/or that their strength is too low to be detected by pyridine at 150 ºC. Overall, these results are in good agreement with those reported for the equivalent Hf-Zn catalyst in the work by De Baerdemaeker et al. [25].

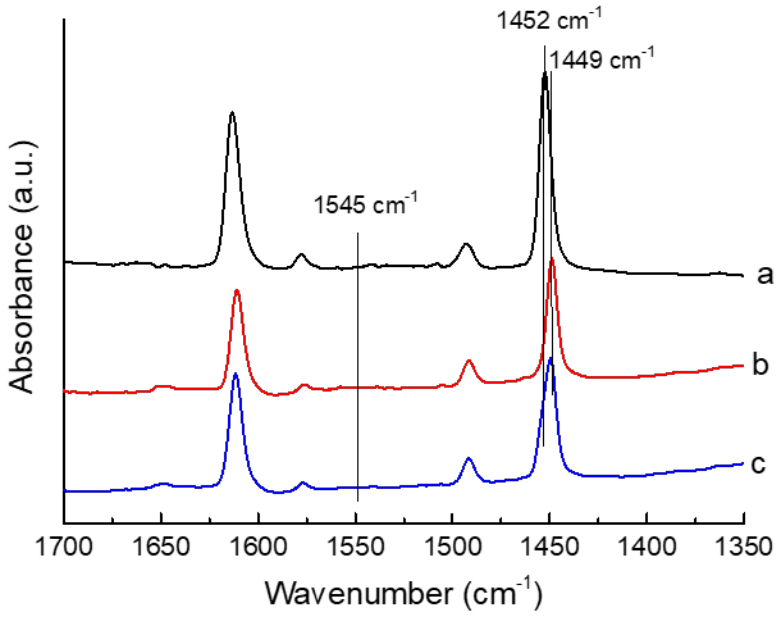

Figure 1. Normalized FTIR-pyridine spectra recorded at a desorption temperature of 150 ºC for HM (a), Hf/SiO_2 (b), and Hf-Zn catalyst (c).

In order to better discern the presence of both Lewis and Brønsted acid sites in the Hf-Zn catalyst and its individual components, we also performed low temperature (-170 ºC) FTIR spectroscopy of CO adsorption, where the C-O stretching frequency of the CO probe molecule is

highly sensitive to the nature and strength of the surface acid sites [47]. The FTIR-CO spectra at increasing CO doses are presented in Fig. S3, where the presence of two main bands at 2190-2188 cm^{-1} and 2159-2152 cm^{-1} assigned to CO adsorbed on surface Lewis (e.g. Hf^{4+} and Zn^{2+} species) and Brønsted (-OH groups) acid sites, respectively, is clearly noticed [47-49]. A more detailed information on the nature and strength of the acid sites can be obtained by analysing the FTIR-CO spectra at low CO doses (i.e. low surface coverages) where dipole-dipole interaction effects are absent, enabling the resolution of several components. Thus, as shown in panel A of Fig. 2, mainly the Lewis acid sites are titrated at 0.1 mbar of CO. The zinc silicate hemimorphite (HM) shows a main band at 2195 cm^{-1} and a less intense one at 2209 cm^{-1} (spectrum a), while only a band at 2195 cm^{-1} is seen for Hf/SiO_2 (spectrum b). The presence of the IR band at a higher frequency (2209 cm^{-1}) in the hemimorphite indicates that this material contains some Lewis acid sites of a higher strength than those present in Hf/SiO_2, as also suggested from the FTIR-pyridine results (Fig. 1). In turn, the Hf-Zn catalyst (spectrum c) exhibits a weak feature at 2195 cm^{-1} besides a more intense peak at 2190 cm^{-1}. The lower frequency of the later band signs for a lower overall strength of the Lewis acid sites in Hf-Zn catalyst relative to HM and Hf/SiO_2. On the other hand, the presence of OH groups (i.e. Brønsted acid sites) of different acid strength becomes clearer at a slightly higher CO coverage of 0.3 mbar, as shown in panel B of Fig. 2. Hence, the hemimorphite presents three bands at 2159, 2151, and 2141 cm^{-1} (spectrum a) while Hf/SiO_2 exhibits a main band at a higher frequency of 2167 cm^{-1} (spectrum b), evidencing that the later sample contains stronger Brønsted acid sites. Although these four bands are also present in Hf-Zn catalyst (spectrum c), the prevailing contribution of the peak at 2159 cm^{-1} suggests a decrease in the average strength of the Brønsted acid sites in the catalyst compared to Hf/SiO_2. Therefore, even if both Lewis and Brønsted acid sites are unambiguously detected in the samples

by FTIR-CO, the results at low CO coverages clearly sign for a lower average strength of both types of acid sites in the Hf-Zn catalyst compared to the individual components. This fact is probably due to interactions arising during the physical mixing of the HM and Hf/SiO_2 components at the catalyst preparation stage.

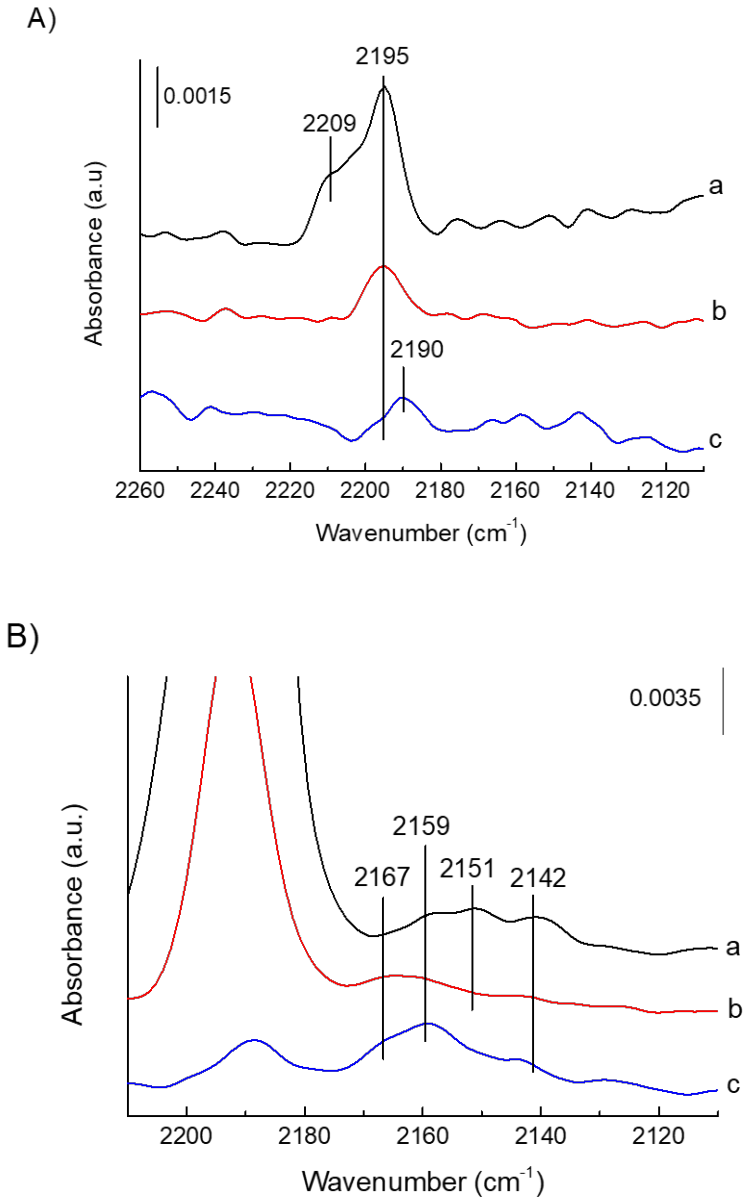

Figure 2. FTIR spectra of CO adsorption (-170 °C) recorded at a CO pressure of 0.1 mbar (panel A) and 0.3 mbar (panel B) for HM (a), Hf/SiO_2 (b), and Hf-Zn catalyst (c) The bands in the

Lewis acid sites region (2195-2188 cm^{-1}) for Hf/SiO_2 and HM in panel B are out of scale.

3.2. Study of the reaction pathway in the ethanol to 1,3-butadiene conversion

In order to study the reaction scheme of 1,3-butadiene formation from ethanol, kinetic curves encompassing a wide range of ethanol conversions (~ 20% - 90%) were obtained for the main products, enabling them to be classified according to their primary/secondary and stable/unstable nature [50]. The full data about ethanol conversions and product yields at 360 ºC, 0.21 bar of ethanol (1 bar total pressure), and variable WHSV are gathered in Table S1. We must note that a direct comparison of the catalytic performance of our catalyst with that of the equivalent catalyst reported in the original work by De Baerdemaeker et al. [25] is not straightforward. This arises mainly from the much higher ethanol partial pressure employed in our study (0.21 against ~0.025 bar) in order to reproduce more closely the operation of an industrial reactor at atmospheric pressure. In general, lower butadiene selectivity is achieved in the present work, as a consequence of a much larger formation of heavy products than reported by De Baerdemaeker et al. [25] for the same reaction temperature and ethanol conversion. This difference in performance is not critical as the purpose of the present work is to determine qualitatively the effects of recycling by-products and catalyst regeneration by calcination.

3.2.1. Reaction path for 1,3-butadiene formation

The kinetic curves for 1,3-butadiene, acetaldehyde, and crotonaldehyde are given in Fig. 3. The shape of the curves is similar to those obtained by Sushkevich et al. [8] over $Ag/ZrO_2/SiO_2$ and by Shylesh et al. [1] over $Au/MgO\text{-}SiO_2$. As seen in Fig. 3, acetaldehyde is the main side product of the ethanol-to-1,3-butadiene reaction. The acetaldehyde yield-conversion curve resembles that of a primary unstable product, indicating that it is directly

generated by the dehydrogenation of ethanol on Lewis acid sites associated to Zn^{2+} species in the hemimorphite [25]. In order to study in which reactions acetaldehyde is involved, a set of tests was carried out feeding pure acetaldehyde (Table S2). As observed, acetaldehyde conversion remained relatively low in all these tests, not exceeding 15% at the lowest WHSV of 1.12 h^{-1}. The main product obtained was crotonaldehyde, plausibly formed by the aldol condensation of acetaldehyde on Lewis acid sites associated with Hf^{4+} species identified in this work by FTIR spectroscopy of adsorbed pyridine (Fig. 1) and CO (Fig. 2). However, almost no traces of 3-hydroxybutanal could be found among the products, probably as a consequence of its rapid dehydration to crotonaldehyde. Carbon monoxide and methane were observed in a mole ratio close to 1:1, except at low acetaldehyde conversion where the mole ratio was 1:2. This suggests that they are mainly formed by the decomposition of acetaldehyde, although other minor sources of methane (more relevant at low acetaldehyde conversions) cannot be discarded. Heavy compounds (C_{6+}) were produced in significant amounts, probably through the self- and cross-condensation of acetaldehyde and crotonaldehyde.

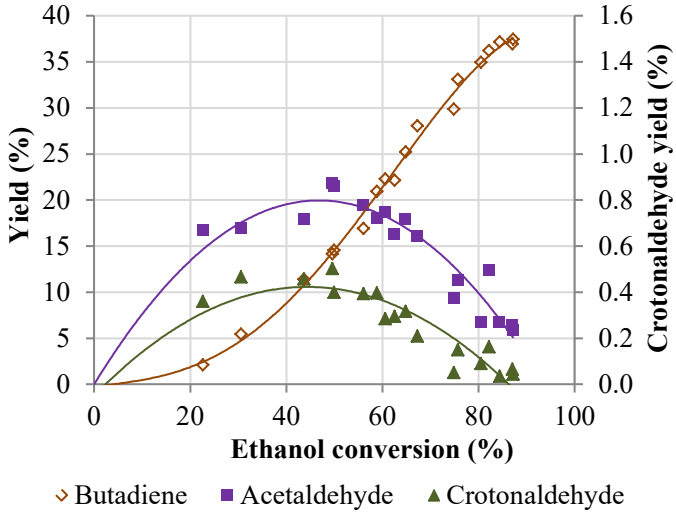

Figure 3. 1,3-butadiene, acetaldehyde, and crotonaldehyde yields as a function of ethanol conversion.

An experiment feeding pure crotonaldehyde was performed in order to study the reactions in which this product is involved. Only qualitative results of this experiment regarding the nature of the species formed will be commented as the large formation of unknown heavy compounds impeded accurately determining the product yields. While the results of this experiment revealed the predominant formation of heavy compounds, supporting their likely formation from crotonaldehyde via self-condensation reactions, no traces of 1,3-butadiene were found among the products. Conversely, an increase in 1,3-butadiene selectivity was observed in experiments co-feeding crotonaldehyde with ethanol (Table S3). This observation supports the pathway suggested in the previous literature where crotyl alcohol was formed through the MPVO reduction of crotonaldehyde with ethanol and subsequently dehydrated to 1,3-butadiene [29,32,36,37,41,51]. In fact, silica-anchored hafnium has proven to be an effective catalyst for the MPV reduction of ketones [52] and alcohols [25] as it forms complexes that favor hydrogen transfer reactions, so we expect MPVO reactions to be promoted by Hf species in the Hf-Zn catalyst.

Almost no crotyl alcohol was detected during the test feeding only ethanol (Table S1), probably due to its high reactivity. The formation of 1,3-butadiene by the dehydration of crotyl alcohol and the rapid rate of this reaction were confirmed by individually feeding crotyl alcohol (Table S4). The conversion of crotyl alcohol at 360 ºC and WHSV of 1.12 $h^{-1}$was 99% with a selectivity of 60% to 1,3-butadiene. Therefore, it can be concluded that, over the Hf-Zn catalyst, both crotonaldehyde and crotyl alcohol are directly involved in the formation of 1,3-butadiene from ethanol, which is in agreement with the most widely accepted reaction pathway ~~(Fig. 1)~~. Indeed, the kinetic curve of 1,3-butadiene (Fig. 3) resembles that of a secondary stable product.

Its stable character was confirmed by the absence of reaction in an additional experiment performed feeding only 1,3-butadiene (Table S5). Similarly, no signs for the occurrence of reactions were evidenced when butadiene was co-fed with ethanol (Table S6).

3.2.2. Formation of by-products

Although ethene and diethyl ether are undesired primary products formed, in theory, by the dehydration of ethanol catalyzed by Brønsted acid sites, there is some controversy in the literature about whether ethene is directly generated by the dehydration of either ethanol or diethyl ether or even from both [8,27,31,53,54]. According to the kinetic curves of diethyl ether and ethene (Fig. 4), they both seem to be primary stable products, suggesting that ethene is not produced from diethyl ether. As the kinetic curve of ethene rises exponentially, there must be another reaction, besides ethanol dehydration, which leads to ethene that does not involve the participation of diethyl ether. Furthermore, the Prins condensation route, whereby 1-3 butadiene is formed by reaction of ethylene with acetaldehyde [38], is ruled out over this catalyst as ethene and diethyl ether are not intermediate products of this reaction. This hypothesis was confirmed in separate experiments co-feeding ethanol and diethyl ether (Table S7), where a nearly constant selectivity (and yield) to 1,3-butadiene and ethene was observed when the concentration of diethyl ether in the feed mixture was increased from 2.5 to 10 wt%. Furthermore, as diethyl ether inlet concentration increases, there is a point where diethyl ether formation from ethanol is suppressed, which could be expected due to the low chemical equilibrium constant of this reaction at the reaction temperature [55].

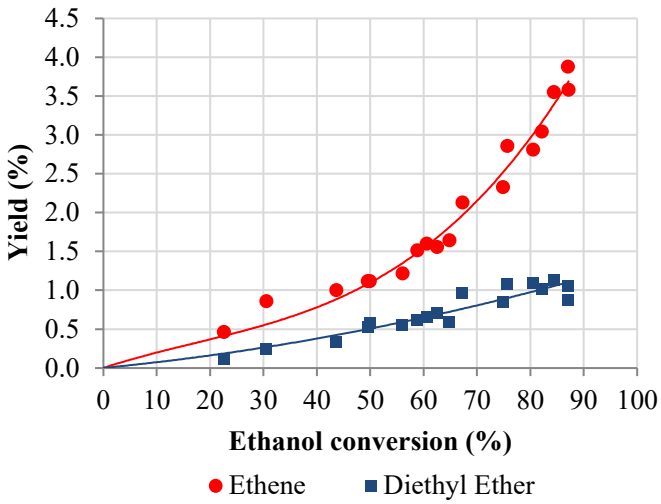

Figure 4. Ethene and diethyl ether yields vs ethanol conversion.

Among the main sub-products, C_4 compounds (1-butanol, butanal, and butenes) represent an important fraction. The sources of 1-butanol and butanal, however, remain to be clarified. Proposed routes leading to 1-butanol include the hydrogenation of butanal, crotonaldehyde or crotyl alcohol [8,29] and the direct condensation of ethanol [15]. Butanal, on the other hand, may be produced through the isomerization of crotyl alcohol, reduction of crotonaldehyde, and the dehydrogenation of 1-butanol [8,29,39]. The kinetic curve of 1-butanol (Fig. 5) clearly exhibits the characteristic shape of a secondary unstable product. Although the curve of butanal also resembles that of a secondary unstable product, this seems less clear than for 1-butanol, as a net decrease in butanal yield above a certain conversion cannot be unambiguously concluded (Fig. 5). The fact that at low ethanol conversions (< 30%) 1-butanol is detected in the products, but not butanal, may be an indication of the dehydrogenation of 1-butanol as a plausible route leading to butanal. This assumption is compatible with the results obtained in an experiment feeding only 1-butanol (Table S8), where butanal was the main product formed, especially at low 1-butanol conversions (butanal selectivity of 68% at 21% conversion), followed by butenes. Since butanal

is formed from 1-butanol, crotonaldehyde hydrogenation should play a minor role as a source of butanal. Then, it seems that crotonaldehyde is mainly hydrogenated to crotyl alcohol by the MPVO reaction, which then can be further hydrogenated to 1-butanol. In fact, when only crotyl alcohol was fed (Table S4), the lumped selectivity to butanol and butenes, as a gross measure of 1-butanol formation, was significant. This indicates that over silica doped metal catalysts, and in the absence of an external H_2 source, 1-butanol likely comes from crotyl alcohol hydrogenation by H fragments present on the catalyst surface originating from previous alcohol dehydrogenations [8,29]. In this respect, Hayashi et al. [24] observed an increase in the selectivity to acetaldehyde, 1-butanol, butanal, and butenes when the Zn content is increased in a Zn/talc catalyst, suggesting that H species generated by ethanol dehydrogenation on Zn sites are responsible for the hydrogenation of crotyl alcohol to 1-butanol, from which butanal and butenes are subsequently formed. Finally, the total butene fraction comprising 1-butene, isobutene, and cis- and trans-2-butene shows the characteristic kinetic curve of a secondary stable product (Fig. 5) which, as discussed before, is in line with a route involving the dehydration of 1-butanol to 1-butene and its successive isomerization to *cis*- and *trans*-2-butene and isobutene [3].

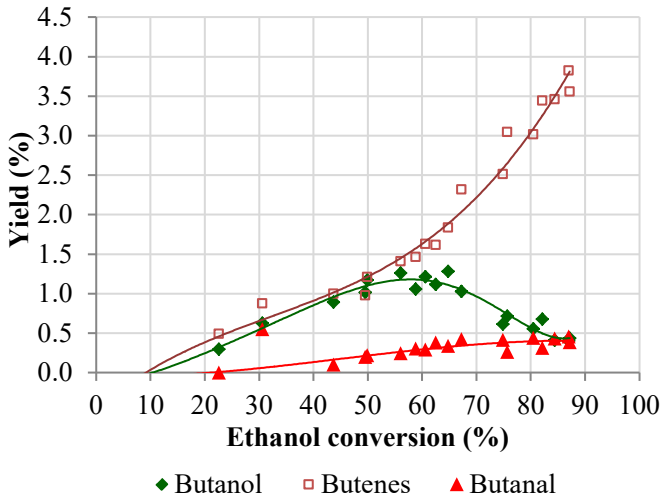

Figure 5. Yields of 1-butanol, butenes, and butanal vs ethanol conversion.

The kinetic curve of ethyl acetate (Fig. 6) indicates that it is a secondary unstable product, probably formed from acetaldehyde by the Tischenko reaction. Indeed, ethyl acetate was observed in the products of the experiment performed feeding only acetaldehyde, albeit in relatively low selectivity (Table S2). Sushkevich et al. [8] have proposed that the further transformation of ethyl acetate leads to acetic acid, which produces acetone through the release of CO_2 by decarboxylation. Finally, acetone can be reduced and dehydrated to propene. This reaction sequence is consistent with the shape and position of the kinetic curves of ethyl acetate, acetone, propene, and CO_2, as depicted in Fig. 6. Acetic acid was observed in trace amounts as it is rapidly transformed into acetone and CO_2 is released. The formation of propene from acetone was confirmed in an experiment feeding pure acetone (not shown), where isopropanol and heavy compounds (C_{6+}) were also found as main products, and in experiments co-feeding ethanol and acetone (Table S9), where the yield of propene was seen to increase with the acetone content in the feed. Besides acetone, the decarbonylation of crotonaldehyde is another plausible source of propene, as inferred from the results of an experiment feeding only crotonaldehyde (not shown).

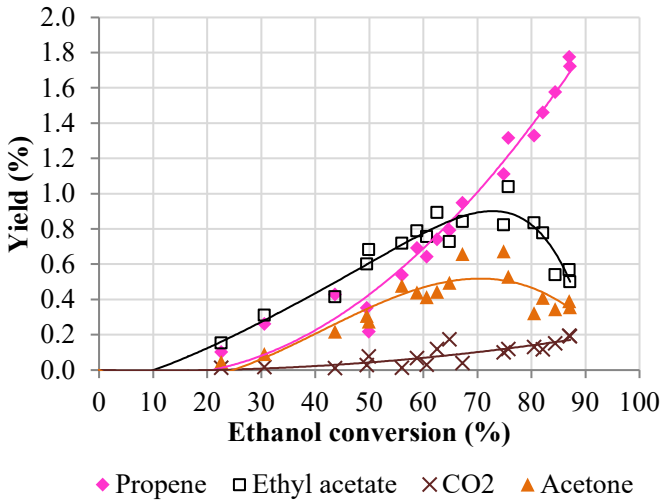

Figure 6. Yields of ethyl acetate, acetone, propene, and CO_2 vs ethanol conversion.

In addition, heavy compounds with more than six carbon atoms (C_{6+}) were produced in significant amounts when feeding pure ethanol (Table S1). The kinetic curve of C_{6+} compounds unambiguously indicates their secondary and stable nature (Fig. 7). Some heavy products can be formed by the self and cross condensation of aldehydes such as crotonaldehyde and butanal, as can be observed in the experiments performed by feeding these compounds (Tables S3 and S10). Indeed, feeding only butanal (not shown) lead to 2-ethyl-2-hexenal as the main product via self-aldol condensation. Moreover, when butanal was co-fed with ethanol (Table S10), the selectivity to heavy compounds increased significantly from ca. 13 to 20% when the concentration of butanal in the feed mixture was raised from 2.5 to 10 wt%, as expected. Other minor by-products like acetone have also proven to contribute to the formation of heavy compounds (Table S9). The deposition of heavy compounds on the Hf-Zn catalyst during the course of the ethanol-to-1,3-butadiene reaction may certainly contribute to its deactivation, as will be discussed in the next section.

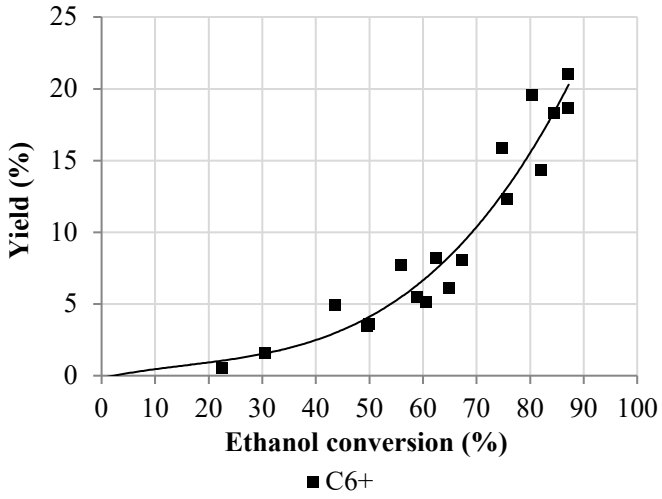

Figure 7. Yield of heavy compounds (C_{6+}) vs ethanol conversion.

As a summary of the experimental observations discussed above, a detailed reaction scheme accounting for the formation of 1,3-butadiene and the side products from ethanol over the Hf-Zn catalyst is shown in Fig. 8.

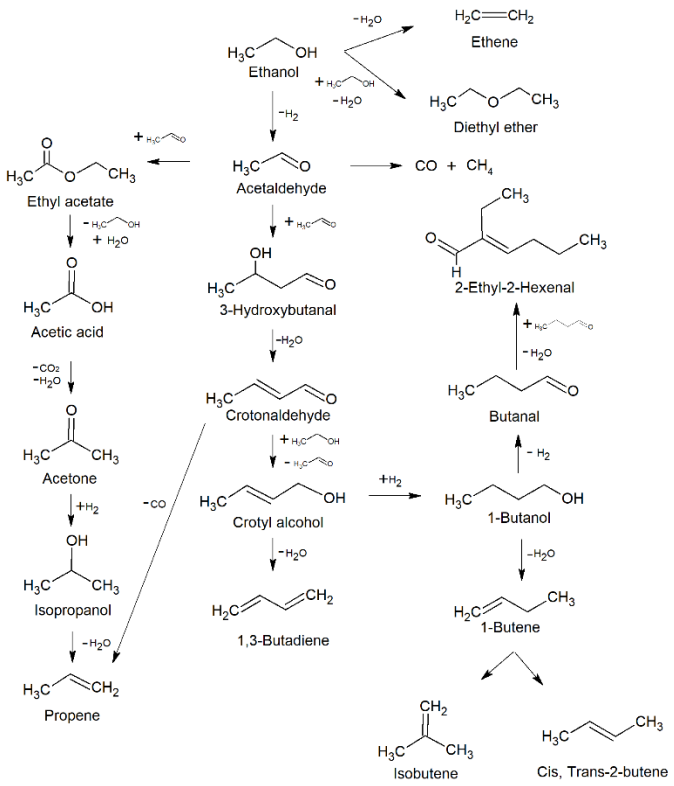

Figure 8. Proposed reaction pathway for the formation of 1,3-butadiene and side products from ethanol over the Hf-Zn catalyst.

3.3. Catalyst deactivation and regeneration

3.3.1. Deactivation-regeneration behaviour

In order to study the deactivation behaviour and regeneration of the Hf-Zn catalyst, a test lasting in total 100 h with two intermediate in-situ regenerations was performed according to the experimental procedure detailed in section 2.3. The evolution with the time-on-stream (TOS) of the ethanol conversion and the yield and selectivity to 1,3-butadiene, acetaldehyde, and ethene+diethyl ether is presented in Fig. 9. As observed, catalyst deactivation resulting in a gradual loss of ethanol conversion with TOS occurred from the beginning of the reaction as well as after regeneration. In turn, the decrease in conversion is accompanied by a progressive

increase in acetaldehyde selectivity and a slight decrease in 1,3-butadiene selectivity, which is more evident in the period following the second regeneration cycle. Moreover, the combined selectivity to dehydration products (ethene+diethyl ether) slightly increased after the regenerations but remained nearly unaltered with TOS within each reaction period. Similar trends in activity and selectivity during the ethanol-to-1,3-butadiene conversion were observed by Baylon et al. [23] in a study reporting the deactivation and regeneration by calcination of a Na-doped Zn-Zr-mixed oxide catalyst. According to these authors, the change in 1,3-butadiene and acetaldehyde selectivity was related to the loss of active sites involved in the conversion of acetaldehyde to 1,3-butadiene.

As seen in Fig. 9, the catalyst recovered most of its initial activity after the two regenerations by calcination in flowing air at 500 ºC. It is worth noting that the activity recovery was somewhat higher after the second regeneration lasting 8 h in contrast to the 6 h applied in the first regeneration cycle. The almost complete recovery of catalyst activity upon calcination in air points to the deposition of coke as a major source of deactivation of the Hf-Zn catalyst.

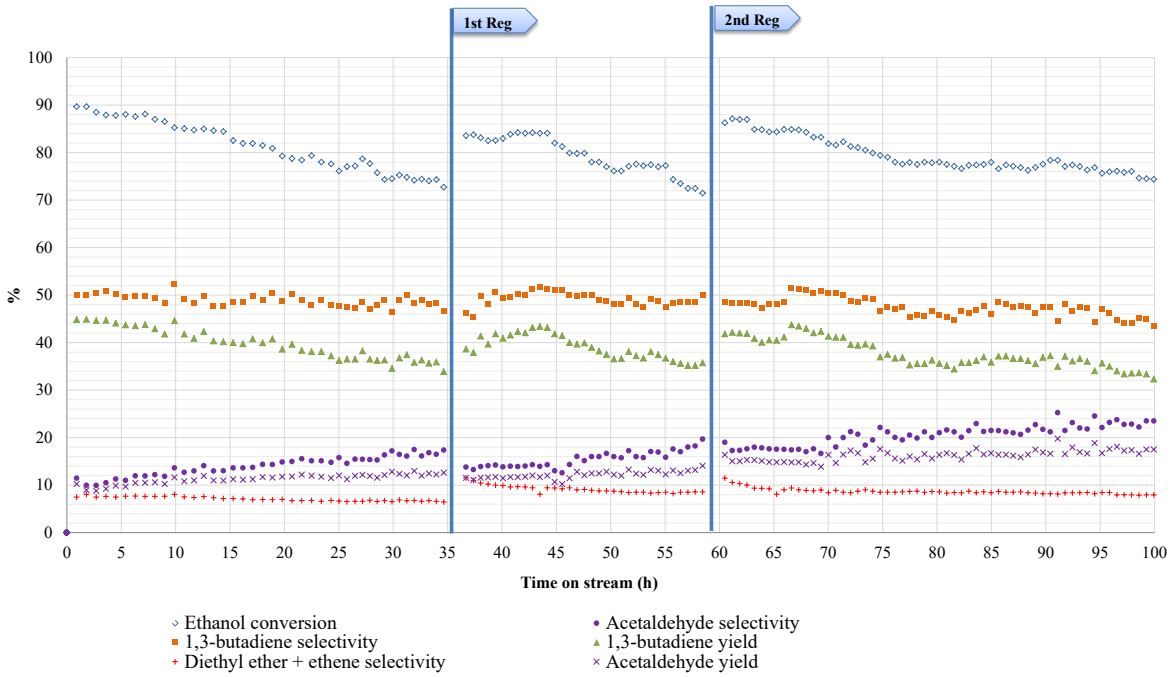

Figure 9. Effect of deactivation on ethanol conversion, main product selectivities and yields. Operating conditions: WHSV= 1.12 $g_{EtOH}/(g_{cat}\cdot h)$, T= 360 ºC, P_{EtOH} of 0.21 bar and P of 1bar. Regenerations were carried out at 500 ºC with air flow of 15 cm^3/min. First and second regenerations lasted 6 and 8 hours, respectively.

3.3.2. Analysis of coke species

With the aim of determining the origin of the observed catalyst deactivation and changes in selectivity, the Hf-Zn catalyst was characterized by different techniques in its fresh state ($HfZn_{fresh}$), after its use in the reaction during the first 35 h on stream ($HfZn_{used}$), and after the second regeneration step ($HfZn_{regen}$). The total carbon contents, measured by the elemental analysis, amounted to 2.56 and 0.17 wt% for the spent and regenerated samples, respectively. This indicates that calcination in air at 500 ºC is effective in removing most of the carbon species from the catalyst and provides support for coke deposition as a main source of deactivation. The

fact that still some carbonaceous material remained in the catalyst after regeneration could explain the slightly lower initial conversion observed after the regeneration cycles with respect to the fresh sample. In fact, the TGA-DTG analysis in air of the used sample (Fig. S4) indicated that part of the carbon deposits could only be removed at temperatures well above 500 ºC.

The nature of the carbon species present in the used sample was investigated by ^{1}H-to-^{13}C CP-MAS NMR spectroscopy and by the extraction of the coke with dichloromethane after the dissolution of the solid in HF, and further analysis by GC-MS. The^{1}H-to-^{13}C CP-MAS NMR spectrum (Fig. 10a) shows two intense, sharp bands at 16 and 59 ppm and three broad components peaking at 76, 127, and 178 ppm. The sharp bands with chemical shifts of 16 and 59 ppm are attributed, respectively, to the methyl carbon (CH_3-) and to the carbon linked to the -OH group of ethanol [56], indicating that part of the carbon retained on the catalyst after the reaction is associated with the ethanol that remained adsorbed on the catalyst. On the other hand, the broad resonance with a maximum located at 127 ppm and the associated spinning side bands at 76 and 178 ppm are characteristic of aromatic carbons [57]. These results are compatible with those reported by Cavani et al. [39], who detected signs of ethanol, aldehydes, and aromatic compounds adsorbed on a MgO catalyst after the ethanol-to-1,3-butadiene reaction by DRIFTS and mass spectrometry. On the other hand, the GC-MS analysis of the coke extracted with dichloromethane confirmed the aromatic nature of the formed carbon species. The most probable structures (> 80% probability) for four of the main compounds detected are shown in Fig. 10b. Therefore, we postulate that the formation and adsorption of relatively bulky oxygenated aromatic species are responsible, at least in part, for the deactivation observed for the Hf-Zn catalyst in the one-step conversion of ethanol to 1,3-butadiene.

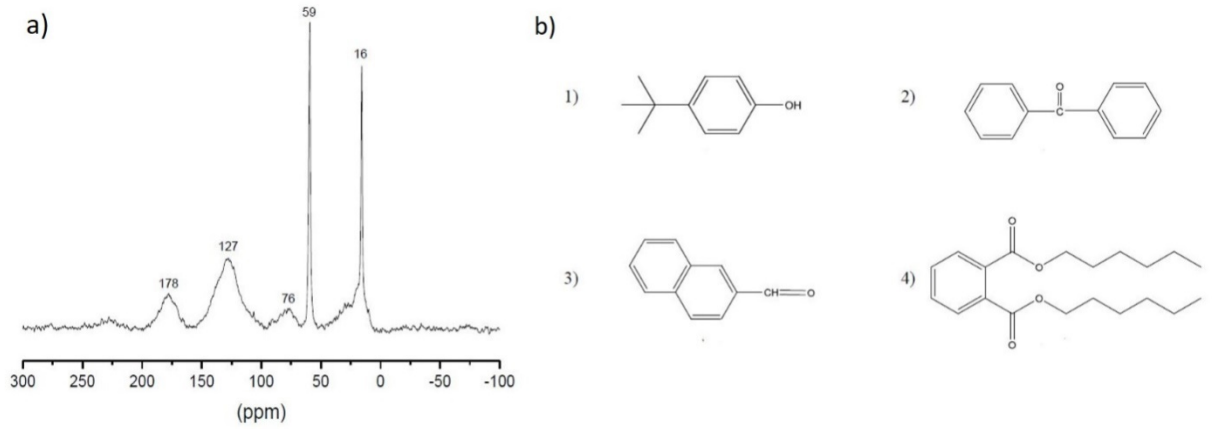

Figure 10. a) Solid-state ^{1}H-to-^{13}C CP-MAS NMR spectrum of spent Hf-Zn catalyst ($HfZn_{used}$); b) main carbonaceous species detected by GC-MS in the coke extracted from $HfZn_{used}$: 1) 4-tert-butylphenol, 2) diphenylketone, 3) 2-naphtaldehyde, and 4) dihexyl phthalate.

3.3.3. Structural and surface characterization of used catalyst

Structural changes in the crystalline hemimorphite (HM) phase in the Hf-Zn catalyst after its use in the reaction and after regeneration were studied by X-ray diffraction (XRD). As shown in Fig. S5a, the crystalline structure of HM was retained after the reaction and regeneration, although a decrease in the intensity of the hemimorphite-related peaks was noticed for the regenerated sample. This loss in crystallinity points to a partial amorphization of the HM phase during the regenerations. In order to confirm this, the fresh Hf-Zn catalyst sample was submitted to two consecutive calcinations in flowing air at 500 ºC for 6 and 8 h, respectively, mimicking the conditions applied in the two in-situ regeneration treatments. As in the case of $HfZn_{regen}$, a decreased intensity of the HM peaks relative to those in the fresh sample was observed after the two calcinations (Fig. S5b), supporting the partial damage to the crystalline structure of hemimorphite during the in situ regeneration treatments. In the original work by De Baerdemaeker et al. [25], it was demonstrated that using hemimorphite as source of Zn^{2+} species

is more effective in promoting the selective formation of 1,3-butadiene and in suppressing unwanted side reactions on Hf-related acid sites compared to Zn^{2+} species generated from a Zn nitrate precursor. Therefore, the loss of the HM phase during the regeneration may expectedly induce an imbalance between Hf and Zn sites in the Hf-Zn catalyst that might account for, at least in part, the changes in activity and selectivity observed during the post-regeneration reaction periods (Fig. 9).

The nature of the surface Hf, Zn, and C species in the fresh, used, and regenerated catalyst was studied by X-ray photoelectron spectroscopy (XPS). Fig. 11 shows the survey XP spectra and the spectra in the Zn2p, Hf4f, and C1s regions. The survey spectra (Fig. S6a) exhibit characteristic peaks at 103, 153, and 533 eV that are attributed to Si2p, Si2s and O1s, respectively [58]. The signals corresponding to Zn2p ($Zn2p_{1/2}$ and $Zn2p_{3/2}$) are located in the region of the spectrum comprised between 1023 and 1046 eV [25,58], while the small peak around 18-19 eV is assigned to the Hf4f core level signal which, due to spin-orbit effects, splits into two peaks at 17.6 and 19.3 eV corresponding, respectively, to the $Hf4f_{7/2}$ (main peak) and $Hf4f_{5/2}$ components [59,60].

a)

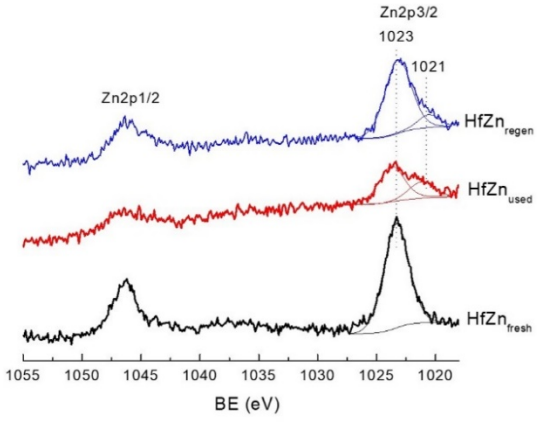

b)

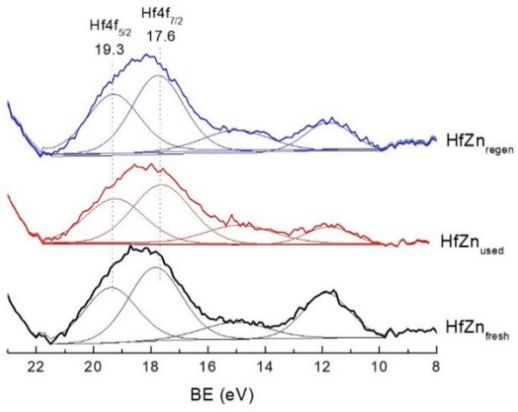

Figure 11. XPS spectra for the Hf-Zn catalyst in its fresh state ($HfZn_{fresh}$), after reaction ($HfZn_{used}$), and after regeneration ($HfZn_{regen}$): a) Zn2p, and b) Hf4f regions.

The XPS spectrum in the Zn2p region (Fig. 11a) of the fresh catalyst exhibits a main $Zn2p_{3/2}$ band at a binding energy (BE) of ca. 1023 eV and a less intense $Zn2p_{1/2}$ signal at 1046 eV which were attributed to the Zn^{2+} species in the crystalline hemimorphite structure. Interestingly, the spectrum of the used sample reveals the contribution to the $Zn2p_{3/2}$ peak of an additional signal at lower BE (1021 eV) assigned to metallic Zn species (Zn^0) [59]. The contribution of the Zn^0 species in $HfZn_{used}$ was estimated to be ca. 34% by deconvolution of the $Zn2p_{3/2}$ peak, indicating a reduction of a significant part of the Zn^{2+} species in the original hemimorphite phase to Zn^0 during the ethanol-to-1,3-butadiene reaction. The reduction of Zn^{2+} to Zn^0 would thus represent a loss in active sites and, thus, an additional source of deactivation, as has also been reported for ZnO during its use as catalyst in dehydrogenation reactions [61,63]. On the other hand, the lower intensity of the peaks in the Zn2p spectrum of $HfZn_{used}$ in comparison to the other samples (Fig. 11a) can be related to the deposition of carbon species on the catalyst surface. It is also seen in Fig. 11a that the regeneration of the used catalyst by calcination at 500 ºC caused the re-oxidation of some Zn^0 species back to Zn^{2+}, with a concomitant decrease in the relative concentration of Zn^0 from 34 to 11%. The reduction of Zn^{2+} is expected to result in the segregation of zinc from the HM structure as Zn^0. Therefore, the re-oxidation of Zn^0 during regeneration is anticipated to result also in the formation of a segregated ZnO phase, whose characteristic $Zn2p_{3/2}$ peak would be expected at a BE of 1022 eV [59] and, thus, hard to be differentiated from the peak of Zn^{2+} in HM (BE= 1023 eV). As discussed in the work by De Baerdemaeker et al. [25] and supported by the acidity results concluded by our FTIR

study, Zn^{2+} cations in HM neutralized most of the Brønsted acid sites associated with Hf-OH groups (generated by hydrolysis on Hf^{4+} species), reducing the formation of dehydration side products (e.g. ethene) while promoting 1,3-butadiene. Considering this, it seems plausible that the transformation of some Zn^{2+} species in the hemimorphite into Zn^0/ZnO during catalysis and regeneration would impair the balance between the different types of active sites (redox, acid/base) in the Hf-Zn catalyst, thus worsening its catalytic performance. Therefore, the loss in hemimorphite-related Zn^{2+} centres would make Hf^{4+} sites less effective for the aldol condensation step while promoting ethanol dehydration, presumably on Hf-OH sites not neutralized by Zn^{2+}. This might account for the increase in selectivity to acetaldehyde and, to a lesser extent, to ethene+diethyl ether in detriment of the 1,3-butadiene observed during the deactivation test (Fig. 9) [61,62].

On the other hand, the XP spectrum of $HfZn_{fresh}$ in the Hf4f region shows a main peak of $Hf4f_{7/2}$ at ca. 17.6 eV (Fig. 11b) which is consistent with Hf^{4+}species in HfO_2 interacting with silica [56-58]. Unlike Zn, the Hf4f XP spectra for $HfZn_{used}$ and $HfZn_{regen}$ were very similar to that of $HfZn_{fresh}$ (Fig. 11b) and, therefore, it is concluded that the oxidation state and the nature of the Hf species remain the same (i.e. HfO_2) during the course of the catalytic reaction and after regeneration.

The nature of the surface carbon species was studied by analyzing the XP spectra of the samples in the C1s region (Fig. S6b). The fresh sample presents C1s bands related to adventitious carbon, as commonly found in XPS analyses. The de-convoluted spectrum of the spent catalyst ($HfZn_{used}$) shows a main component at 284.5 eV that can be attributed to either aliphatic or aromatic carbons [63-65]. An additional component at 285.9 eV, characteristic of carbon linked to oxygen in C-O-H and C-O, is also evidenced, while the contribution at 287.7 eV

could be associated with C=O [67]. These features are essentially in agreement with the nature of the CH_2Cl_2-soluble coke species determined by GC-MS (Fig. 10b).

Table 4 shows the surface composition of the catalyst in its different states as determined by XPS. It can be seen that the carbon content on the catalyst surface almost doubles after reaction, consistent with the deposition of carbonaceous compounds also inferred from the previous characterizations. As a result, the surface concentration of Zn and Si in $HfZn_{used}$ decreased by 50% and 40%, respectively, with respect to $HfZn_{fresh}$, while the concentration of Hf was much less affected (15% decrease). This suggests that the aromatic-type carbonaceous species were preferentially formed and retained on the dehydrogenating Zn^{2+} species in the hemimorphite component of the catalyst. After regeneration of the catalyst, the surface contents of Zn, Si, and Hf increased, approaching the values of the fresh catalyst. Concomitantly, the amount of carbon decreased to levels close to those in the fresh sample, supporting the removal of most of the coke from the catalyst after regeneration by calcination in air at 500 ºC.

Table 4. Atomic surface composition and metal surface ratios determined by XPS.

	Atomic surface concentration (%)				Surface atomic ratios		
Catalyst	Zn	Hf	Si	C	Zn/Hf	Zn/Si	Hf/Si
$HfZn_{fresh}$	0.50	0.20	32.0	24.3	2.6	0.015	0.006
$HfZn_{used}$	0.25	0.17	19.3	40.0	1.4	0.013	0.009
$HfZn_{regen}$	0.40	0.19	23.5	29.4	2.1	0.017	0.008

Finally, representative STEM images and element EDX maps (Si, Zn) for the used and regenerated Hf-Zn samples are shown in Figs. S7a and S7b, respectively. No noticeable changes

in the dispersion of Zn species with respect to the fresh sample ($HfZn_{fresh}$, Fig. S2) were inferred from this technique after catalysis ($HfZn_{used}$) and after regeneration ($HfZn_{regen}$).

4. Conclusions

The one-step ethanol to 1,3-butadiene pathway was studied over a Hf-Zn catalyst prepared as physical mixture of Hf/SiO_2 and zinc silicate hemimorphite (HM). The mixed Hf-Zn catalyst was seen to possess mainly Lewis-type acidity, as ascertained by FTIR spectroscopy of adsorbed pyridine. Nonetheless, both Lewis and Brønsted acid sites of different strengths associated with Zn and Hf species in the hemimorphite and Hf/SiO_2 solids, respectively, were detected by low-temperature FTIR of CO adsorption, a more surface-sensitive technique. According to FTIR-CO, the hemimorphite phase contained stronger Lewis acid sites than Hf/SiO_2 while the later solid exhibited stronger Brønsted acid sites. Interestingly, the average strength of both types of acid sites decreased upon physically mixing the two phases during the preparation of the Hf-Zn catalyst. Kinetic curves were evaluated in a wide range of ethanol conversions and allowed for elucidating the main reactions leading to 1,3-butadiene and by-products. In addition, several intermediate compounds have been fed or co-fed with ethanol to assess some of the intermediate steps. Our results support the generally accepted pathway to 1,3-butadiene: ethanol dehydrogenation to acetaldehyde, acetaldehyde aldol-condensation to crotonaldehyde, crotonaldehyde reduction with ethanol, and crotyl alcohol dehydration. Regarding side products, ethene and diethyl ether seem to be primary stable products formed from ethanol. The decarbonylation of aldehydes has been observed over the catalyst: acetaldehyde to methane and crotonaldehyde to propene, with the concomitant release of carbon monoxide. Ethyl acetate is likely produced via the Tishchenko reaction and then further

transformed into acetone and propene, which releases carbon dioxide. 1-Butanol seems to be formed from crotyl alcohol hydrogenation with surface H fragments originating from previous dehydrogenation reactions. 1-Butanol dehydrogenation and dehydration are the main sources of butanal and 1-butene, respectively. 1-Butene can be isomerized into cis- and trans-2-butenes. The source of heavy compounds appears to be the self- and cross-condensation of C_{4+} aldehydes, like butanal and crotonaldehyde, and ketones, like acetone.

These results give some insight into which by-products should be removed from unreacted ethanol before being recycled into the reactor. The recycling of butanal and acetone should be avoided, as they are finally converted to heavy compounds by aldol condensation reactions. Heavy product formation leads to the deactivation of the catalyst, the fouling of downstream equipment and also makes it difficult to recover and recycle ethanol. Recycling 1-butanol should also be avoided, as its dehydrogenation leads to butanal and then to heavy products while 1-butanol dehydration leads to butenes, which are difficult to separate from 1-3 butadiene due to their similar boiling points, shape and polarity. Finally, the recycling of diethyl ether can suppress unwanted diethyl ether formation from ethanol due to the low equilibrium constant of that reaction at a high temperature. The economic viability of this measure will depend on the cost of separating and recycling diethyl ether and the increase in 1,3-butadiene selectivity due to the suppression of diethyl ether formation.

It has been found that catalyst deactivation in the course of the reaction is mostly caused by the formation and retention of aromatic-type carbonaceous species preferentially on the dehydrogenating Zn^{2+} sites of the hemimorphite phase of the catalyst and by the reduction of some of these Zn^{2+} sites to Zn^{0}. The loss in Zn^{2+} sites induces a misbalance between Hf^{4+} and Zn^{2+} sites which also results in a change in catalyst selectivity. Regeneration by calcination with

air removes coke and re-oxidizes a fraction of Zn^0 back to Zn^{2+}, but it does not completely re-establish the Zn^{2+}/Hf^{4+} site balance as the re-oxidized Zn species are segregated from the original hemimorphite phase and provide a less favorable interaction with Hf sites.

5. Acknowledgements

This work was carried out in the framework of the project "Biobutadiene production from bioethanol" (CTQ2015-71427-R), which is funded by the Spanish Ministry of Economy, Industry and Competitiveness (MINECO) through the European Regional Development Fund (ERDF). The authors would like to thank Maria Jesús Plumed Freire (US) for her invaluable collaboration, support and dedication in conducting the catalytic tests, and to Dr. Patricia Concepción (ITQ, Valencia) for her assistance in the FTIR-CO study.

6. References

[1] S. Shylesh, A.A. Gokhale, C.D. Scown, D. Kim, C.R. Ho, A.T. Bell, ChemSusChem 9 (2016) 1462–1472.

[2] A.J. Nizamoff. On-purpose Butadiene. Report abstract. Chemsystem PERP Program. Nexant. (2013).

[3] E. V. Makshina, M. Dusselier, W. Janssens, J. Degrève, P.A. Jacobs, B.F. Sels, Chem. Soc. Rev. 43 (2014) 7917–7953.

[4] S. Da Ros, M.D. Jones, D. Mattia, J.C. Pinto, M. Schwaab, F.B. Noronha, S.A. Kondrat, T.C. Clarke, S.H. Taylor, ChemCatChem 8 (2016) 2376–2386.

[5] R.A. Flach B., Lieberz A., USDA Foreign Agric. Serv. (2017) 1–44.

[6] REN21, Renewables 2017: Global Status Report, 2017.

[7] C. Angelici, B.M. Weckhuysen, P.C.A. Bruijnincx, ChemSusChem 6 (2013) 1595–1614.

[8] V.L. Sushkevich, I.I. Ivanova, V. V. Ordomsky, E. Taarning, ChemSusChem 7 (2014) 2527–2536.

[9] M.D. Jones, C.G. Keir, C. Di Iulio, R.A.M. Robertson, C. V. Williams, D.C. Apperley, Catal. Sci. Technol. 1 (2011) 267.

[10] B.B. Corson, H.E. Jones, C.E. Welling, J.A. Hinckley, E.E. Stahly, Ind. Eng. Chem. 42 (1950) 359–373.

[11] I. Lebedev, Zh. Obs. Khim 3 (1933) 698–717.

[12] I. Ostromislensky, J. Russ. Phys. Chem. Soc. 47 (1915) 1494.

[13] C. Angelici, M.E.Z. Velthoen, B.M. Weckhuysen, P.C.A. Bruijnincx, ChemSusChem 7 (2014) 2505–2515.

[14] C. Angelici, M.E.Z. Velthoen, B.M. Weckhuysen, P.C.A. Bruijnincx, Catal. Sci. Technol. 5 (2015) 2869–2879.

[15] J.V. Ochoa, C. Bandinelli, O. Vozniuk, A. Chieregato, A. Malmusi, C. Recchi, F. Cavani, Green Chem. 18 (2016) 1653–1663.

[16] S.H. Chung, C. Angelici, S.O.M. Hinterding, M. Weingarth, M. Baldus, K. Houben, B.M. Weckhuysen, P.C.A. Bruijnincx, ACS Catal. 6 (2016) 4034–4045.

[17] X. Huang, Y. Men, J. Wang, W. An, Y. Wang, Catal. Sci. Technol. 7 (2017) 168–180.

[18] Y. Kitayama, M. Satoh, T. Kodama, Catal. Letters 36 (1996) 95–97.

[19] M. Lewandowski, G.S. Babu, M. Vezzoli, M.D. Jones, R.E. Owen, D. Mattia, P. Plucinski, E. Mikolajska, A. Ochenduszko, D.C. Apperley, Catal. Commun. 49 (2014) 25–28.

[20] O. V. Larina, P.I. Kyriienko, S.O. Soloviev, Catal. Letters 145 (2015) 1162–1168.

[21] O. V. Larina, P.I. Kyriienko, V. V. Trachevskii, N. V. Vlasenko, S.O. Soloviev, Theor. Exp. Chem. 51 (2016) 387–393.

[22] V.L. Dagle, M.D. Flake, T.L. Lemmon, J.S. Lopez, L. Kovarik, R.A. Dagle, Appl. Catal. B Environ. 236 (2018) 576–587.

[23] R.A.L. Baylon, J. Sun, Y. Wang, Catal. Today 259 (2016) 446–452.

[24] Y. Hayashi, S. Akiyama, A. Miyaji, Y. Sekiguchi, Y. Sakamoto, A. Shiga, T. Koyama, K. Motokura, T. Baba, Phys. Chem. Chem. Phys. 18 (2016) 25191–25209.

[25] T. De Baerdemaeker, M. Feyen, U. Müller, B. Yilmaz, F.S. Xiao, W. Zhang, T. Yokoi, X. Bao, H. Gies, D.E. De Vos, ACS Catal. 5 (2015) 3393–3397.

[26] M.Y. Kagan, O.M. Lyubarskii, G. D. Podurovskaya, Izv. Akad. Nauk SSSR Ser Khim (1947) 173–181.

[27] W.M. Quattlebaum, W.J. Toussaint, J.T. Dunn, J. Am. Chem. Soc. 69 (1947) 593–599.

[28] W.J. Toussaint, J.T. Dunn, D.R. Jachson, Ind. Eng. Chem. 39 (1947) 120–125.

[29] V.L. Sushkevich, I.I. Ivanova, S. Tolborg, E. Taarning, J. Catal. 316 (2014) 121–129.

[30] M. León, E. Díaz, S. Ordóñez, Catal. Today 164 (2011) 436–442.

[31] H. Niiyama, S. Morii, E. Echigoya, Bull. Chem. Soc. Jpn. 45 (1972) 655–659.

[32] M. Gao, Z. Liu, M. Zhang, L. Tong, Catal. Letters 144 (2014) 2071–2079.

[33] Z. Han, X. Li, M. Zhang, Z. Liu, M. Gao, RSC Adv. 5 (2015) 103982–103988.

[34] W.E. Taifan, T. Bučko, J. Baltrusaitis, J. Catal. 346 (2017) 78–91.

[35] W.E. Taifan, G.X. Yan, J. Baltrusaitis, Catal. Sci. Technol. 7 (2017) 4648–4668.

[36] S.K. Bhattacharyya, J. Catal. 7 (1967) 152–158.

[37] S.K. Bhattacharyya, B.N. Avasthi, Ind. Eng. Chem. Process Des. Dev. 2 (1963) 45–51.

[38] V. Gruver, A. Sun, J.J. Fripiat, Catal. Letters 34 (1995) 359–364.

[39] A. Chieregato, J.V. Ochoa, C. Bandinelli, G. Fornasari, F. Cavani, M. Mella, ChemSusChem 8 (2015) 377–388.

[40] T.W. Kim, J.W. Kim, S.Y. Kim, H.J. Chae, J.R. Kim, S.Y. Jeong, C.U. Kim, Chem. Eng. J. 278 (2015) 217–223.

[41] W. Janssens, E. V. Makshina, P. Vanelderen, F. De Clippel, K. Houthoofd, S. Kerkhofs, J.A. Martens, P.A. Jacobs, B.F. Sels, ChemSusChem 8 (2015) 994–1008.

[42] M.D. Jones, Chem. Cent. J. 8 (2014) 1–5.

[43] P.I. Kyriienko, O. V. Larina, S.O. Soloviev, S.M. Orlyk, C. Calers, S. Dzwigaj, ACS Sustain. Chem. Eng. 5 (2017) 2075–2083.

[44] S. Da Ros, M.D. Jones, D. Mattia, M. Schwaab, F.B. Noronha, J.C. Pinto, Appl. Catal. A Gen. 530 (2017) 37–47.

[45] V.L. Sushkevich, I.I. Ivanova, E. Taarning, Green Chem. 17 (2015) 2552–2559.

[46] J.L. Cheong, Y. Shao, S.J.R. Tan, X. Li, Y. Zhang, S.S. Lee, ACS Sustain. Chem. Eng. 4 (2016) 4887–4894.

[47] K.I. Hadjiivanov, G.N. Vayssilov, Adv. Catal. 47 (2002) 307–511.

[48] C. Morterra, G. Cerrato, V. Bolis, B. Fubini, Spectrochim. Acta Part A Mol. Spectrosc. 49 (1993) 1269–1288.

[49] G. Ghiotti, F. Boccuzzi, R. Scala, J. Catal. 92 (1985) 79–97.

[50] B.W. Wojciechowski, A.-N. Ko, Int. J. Chem. Kinet. 15 (1983) 1249–1274.

[51] G. Natta, R. Rigamonti, Chim. Ind. 29 (1947) 195–200.

[52] F. Quignard, O. Graziani, A. Choplin, Appl. Catal. A Gen. 182 (1999) 29–40.

[53] M. Zhang, Y. Yu, Ind. Eng. Chem. Res. 52 (2013) 9505–9514.

[54] I. Takahara, M. Saito, M. Inaba, K. Murata, Catal. Letters 105 (2005) 249–252.

[55] J.E. Connett, J. Chem. Thermodyn. 4 (1972) 135–138.

[56] S. Radhakrishnan, P.J. Goossens, P.C.M.M. Magusin, S.P. Sree, C. Detavernier, E. Breynaert, C. Martineau, F. Taulelle, J.A. Martens, J. Am. Chem. Soc. 138 (2016) 2802–2808.

[57] M.A. Callejas, M.T. Martínez, T. Blasco, E. Sastre, Appl. Catal. A Gen. 218 (2001) 181–188.

[58] M.P. Pachamuthu, K. Shanthi, R. Luque, A. Ramanathan, Green Chem. 15 (2013) 2158.

[59] S. Yokoyama, K. Tamura, T. Hatta, S. Nemoto, Y. Watanabe, H. Yamada, Clay Sci. 13 (2006) 75–80.

[60] V. Udayakumar, A. Pandurangan, J. Porous Mater. 24 (2017) 979–990.

[61] A. Ramadoss, K. Krishnamoorthy, S.J. Kim, Mater. Res. Bull. 47 (2012) 2680–2684.

[62] K.D. Jung, O.S. Joo, S.H. Han, S.J. Uhm, I.J. Chung, Catal. Letters 35 (1995) 303–311.

[63] G. Liu, L. Zeng, Z.J. Zhao, H. Tian, T. Wu, J. Gong, ACS Catal. 6 (2016) 2158–2162.

[64] B. Lin, J. Wang, Q. Huang, M. Ali, Y. Chi, J. Anal. Appl. Pyrolysis 128 (2017) 291–303.

[65] D. Zhang, R. Wang, L. Wang, X. Yang, J. Mol. Catal. A Chem. 366 (2013) 179–185.

[66] J.F. Moulder, W.F. Stickle, P.E. Sobol, K.D. Bomben, Surf. Interface Anal. (1992) 261.